J. Fluid Mech. (1981), *vol.* 107, *pp.* 37–55
Printed in Great Britain

Visualization of the flow adjacent to a vertical ice surface melting in cold pure water

By VAN P. CAREY AND BENJAMIN GEBHART

Department of Mechanical Engineering, State University of New York at Buffalo, Amherst, NY 14260

(Received 3 June 1980)

Time-exposure photographs of the buoyancy-driven flow adjacent to a vertical ice surface melting in pure water are presented for ambient water temperatures between 3·9 and 8·4 °C. These conditions are of special interest since between about 4 and 8 °C the buoyancy force distribution is locally bi-directional across the thermal transport region, owing to the density extremum at about 4 °C. Although knowledge of the transport for such circumstances is important in both environmental and technological applications, previous experimental studies have provided only limited information, concerning only the gross aspects of the resulting fluid motions. It is now possible, from the extensive experimental results presented here, to understand some of the more subtle mechanisms which arise in such flows. Photographs of the entire flow field document the many complicated flow configurations which occur for these circumstances. As the ambient water temperature is increased from 3·9 to 8·4 °C, regimes of upward, locally bi-directional, and downward flow are observed. Bi-directional flow is seen to result from the reversal of part or all of the upward wake above the top of the ice surface. Local velocities and surface heat-transfer rates, measured from the photographs, are compared, where possible, with the analytical results of Carey, Gebhart & Mollendorf (1980). It was found that the flow velocities for ambient temperatures from 4·05 to 4·70 °C, depart only slightly from the analytical predictions, in spite of an interaction of the outer portion of the upward flow with downward-moving remnants of the upward wake. However, near the surface, the velocity profiles, and consequently the heat transfer and melting rates, agree well with the analytical results. Comparisons at ambient temperatures below 4·05 °C and above 5·9 °C show that the velocity profile and surface heat transfer are in excellent agreement with the results of Carey *et al.* (1980). At ambient water temperatures between 4·7 and 5·0 °C the flow was found to be bi-directional and weakly time dependent. This weak time dependence is attributed to the instability of the upward wake, which in turn is the source of the outside downward flow in such circumstances.

1. Introduction

A number of previous studies have considered vertical natural convection flow in water near the temperature at which the density is a maximum. A summary of these studies is found in Gebhart & Mollendorf (1978) and in Bendell & Gebhart (1976). Of these studies only a few have attempted, either experimentally or analytically, to deal with the range of temperature conditions which result in locally bi-directional buoyancy force and, for some conditions, locally bi-directional flow. This work

considers those thermally driven flows generated adjacent to vertical flat melting ice surfaces.

Gebhart & Mollendorf (1978) have shown that similarity solutions may be obtained for a wide class of such vertical flows in cold water, particularly the one arising adjacent to an isothermal surface. The buoyancy force distribution across the thermal layer was found to depend principally on the parameter $R = (t_m - t_\infty)/(t_0 - t_\infty)$. Here t_m is the temperature of maximum density, t_0 is the surface temperature and t_∞ is the temperature of the ambient water. In particular, if $0 < R < \frac{1}{2}$, the buoyancy force will change direction across the thermal region. In this range of R, the buoyancy force is up near the surface but reverses to downward near the outer edge of the thermal region. Such flows are of special interest because they depart strongly from the conventional boundary-layer behaviour, which occurs for $R \leqslant 0$ and $R \geqslant \frac{1}{2}$. In addition, the resulting Nusselt number in the range $0 < R < \frac{1}{2}$ may be as much as 50% below the values which apply for $R \leqslant 0$ and $R \geqslant \frac{1}{2}$. For ice melting in pure water, $t_0 = 0$ °C. Then, $0 < R < \frac{1}{2}$ corresponds to an ambient temperature range of $4{\cdot}03$ °C $< t_\infty < 8{\cdot}06$ °C, for the density formulation of Gebhart & Mollendorf (1977). Such temperature conditions commonly occur both in freshwater bodies in the environment and in technological applications.

Despite the importance of understanding the resulting transport, no previous study has provided a comprehensive picture of the behaviour of such flows. Recently, Josberger (1979) has studied experimentally the flow adjacent to a vertical ice surface melting in saline water at oceanic salinities. Such flows are even further complicated by the simultaneous opposed buoyancy effects of salinity and temperature differences, resulting in a bi-directional buoyancy force. For water of oceanic salinity these experiments provide considerable information about the resulting complex flow behaviour. However, detailed experimental information is very sparse about the thermally driven flows with buoyancy force reversal due to an extremum. Only four previous studies have examined the complicated velocity profiles which result for R between 0 and $\frac{1}{2}$. The first study, by Schecter & Isbin (1958), presented both analysis and experimental results for natural convection flow adjacent to a vertical heated surface in cold water. An integral boundary-layer technique and a polynomial dependence of density on temperature were used to analyse the conventional boundary-layer flow for $R \leqslant 0$ and $R \geqslant \frac{1}{2}$. With additional assumptions about the flow, an attempt was also made to use the integral technique to analyse the bi-directional flow which resulted for some of the conditions which arise in the range $0 < R < \frac{1}{2}$. Illuminated particles suspended in the water were used to facilitate flow visualization and to measure the velocity at different locations in the flow; heat transfer from the electrically heated surface was also measured. Some of the flow characteristics and typical measured velocity profiles for conditions which resulted in bi-directional flow were also presented. However, no comparison was made between the measured velocities and the results of the integral analysis. Measured heat-transfer results were found to agree well with the predictions of the integral technique for both the conventional boundary-layer and bi-directional flows.

The second study to deal with flows for which $0 < R < \frac{1}{2}$ is that of Vanier & Tien (1968). Using a polynomial dependence of density on temperature, a similarity solution was developed for the laminar, natural convection boundary-layer flow adjacent to a vertical isothermal surface in pure water. For conditions corresponding to

$0 < R < \frac{1}{2}$, solutions with entirely upward flow, solutions with entirely downward flow, and solutions with small flow reversals near the surface were found. Entirely upward flow was found for R near 0. Entirely downward flow was found near $R = \frac{1}{2}$. For conditions corresponding to R near 0·30, solutions for which the flow was up near the surface and down in the outer region of the flow were indicated. Solutions were not obtainable in the range of conditions between these small inside flow reversals and fully upward flow.

In a more recent experimental study, Wilson & Vyas (1979) present measured velocity profiles near a vertical ice surface melting into distilled water. The ice surface in their experiment extends above the horizontal air–water interface. Thus, flow up along the ice surface, upon reaching the interface, must then turn away from the surface and move out along the air–water interface into the ambient. Clearly, the immersion length is an added parameter in this study. A small amount of pH indicator was added to the water and its pH was adjusted to about 8 by titration with NaOH and HCl. To visualize the flow, a 2·2 cm-long wire electrode was positioned normal to the ice surface with the tip of the wire nearly touching the ice. The electrode was then energized, changing the pH of the water close to the wire. This triggered the pH indicator, causing the affected fluid to turn blue. This blue fluid was photographed as it moved with the flow, and velocities parallel to the surface were inferred from the photographs. Velocity measurements were all taken at a location 5 cm from the bottom of the ice surface and 25 cm below the air–water interface in a 32 cm deep tank.

For an ambient water temperature of 2·0 °C, outside the R range of bi-directional buoyancy force, Wilson & Vyas found poor agreement between their measured velocity profile and that from the analysis of Vanier & Tien (1968). It was concluded that this is due to a deficiency in the density correlation used in that analysis. Their measured velocity profiles indicate that, for ambient temperatures less than 4·7 °C, the flow is entirely upward. For t_∞ between 4·7 °C and 7·0 °C they indicate that the flow was bi-directional and oscillating.

While the results of Wilson & Vyas provide considerable new information, some important other aspects of these flows were not explored. The measurements indicate the flow behaviour only within 2·2 cm of the ice surface and only at the single vertical location 5 cm above the lower edge of the ice slab. Features of the flow field farther from the surface or at other vertical locations were not detected. The interaction of the flow with the air–water interface would seem to be important, particularly for the bi-directional and downward flows. Also, for the bi-directional flows, there is no indication of how the upward and downward portions of the bi-directional flows interact at the top and bottom of the ice surface, nor can the mechanism of the reported time-varying behaviour be surmised from their results.

The study by Carey *et al.* (1980) used the precise density correlation of Gebhart & Mollendorf (1977) and the formulation of Gebhart & Mollendorf (1978) to compute similarity solutions for the natural convection flow adjacent to a vertical isothermal surface in cold water for $0 \leqslant R \leqslant \frac{1}{2}$. Carey *et al.* found the flow to be entirely upward for $R < 0{\cdot}15$ and entirely downward for $R > 0{\cdot}32$. For $0{\cdot}292 \leqslant R \leqslant 0{\cdot}32$ the flow was found to be bi-directional. It was not possible to obtain solutions for $0{\cdot}152 \leqslant R < 0{\cdot}292$. These results represent an improvement over those of Vanier & Tien (1968) since a more accurate density relation was used. Also, the formulation is more general and the results may be applied to thermally driven flows in both pure and saline

water. In addition, Carey *et al.* determined the conditions for incipient inside and outside flow reversal, whereas Vanier & Tien found only inside flow reversals. The heat-transfer coefficients predicted by Carey *et al.* were found to be in good agreement with those inferred from the ice-melting experiments of Bendell & Gebhart (1976).

Given the previous studies discussed above, there remained many aspects of the flow behaviour for $0 \leqslant R \leqslant \frac{1}{2}$ which were not well understood. The experimental results of Schecter & Isbin (1958) and Wilson & Vyas (1979) provide a limited picture of the flow behaviour. Boundary-layer theory appears to be valid for some circumstances, but a comparison between experiment and theory has not been made. The present study was therefore undertaken to provide detailed local information about these flows. Specifically, a flow-visualization technique was used to examine the flow adjacent to a vertical ice surface melting in pure water, for a range of ambient water temperatures corresponding to $0 \leqslant R \leqslant \frac{1}{2}$. Photographs of the entire flow field are shown. Local flow velocities have been measured and are compared where possible with the results of the boundary-layer analysis of Carey *et al.* Local heat-transfer data has also been inferred from the local ice-melting rates measured in the photographs. The results provide considerable detailed information about the very complex flows which arise in this range of R.

2. Experiment

In the experiment, an ice slab 18·4 cm wide, 23·2 cm high and initially 3 cm thick was used. The ice was surrounded by 2·5 cm of expanded polystyrene insulation supported by an acrylic plastic 'picture frame' (figure 1). To freeze the ice slab, the insulation and frame assembly was placed in a mould consisting of a shallow aluminium pan with plastic inserts to produce a protruding surface with clean straight edges. The bottom of the mould was a 6 mm thick machined tool plate to ensure a flat ice surface. The mould was filled with de-ionized water which had been vigorously boiled to remove dissolved gases. The mould was then insulated on the top and sides and placed in a freezer, where the water froze from the bottom upward. Any remaining dissolved gas thereby appeared as bubbles near the top surface of the ice.

After freezing, the mould was removed from the freezer and permitted to warm slowly until the ice was completely at the equilibrium temperature of 0 °C. The slab then was removed from the mould. The ice surface which formed at the bottom of the mould was bubble-free and had clean, straight leading, trailing and side edges. Flow along this surface was visualized after insertion in the tank. The other ice surface, although less perfect, also melted during the experiment and provided symmetric wake conditions above and/or below the slab. The ice was moulded so that, when the surface was positioned vertically, the ice slab extended horizontally 9 mm out beyond the insulation and support frame (figure 1). This provided horizontal leading and trailing edges and ensured that the flow near the leading and trailing edges was not strongly affected by the support frame. Embedded in the ice were two 0·013 cm diameter copper–constantan thermocouples to indicate when the ice initially had reached equilibrium at 0 °C. This assured that there was no heat conduction into the interior of the ice slab during the experiment.

The slabs were melted in a glass tank 86 cm deep, 69 cm long and 66 cm wide.

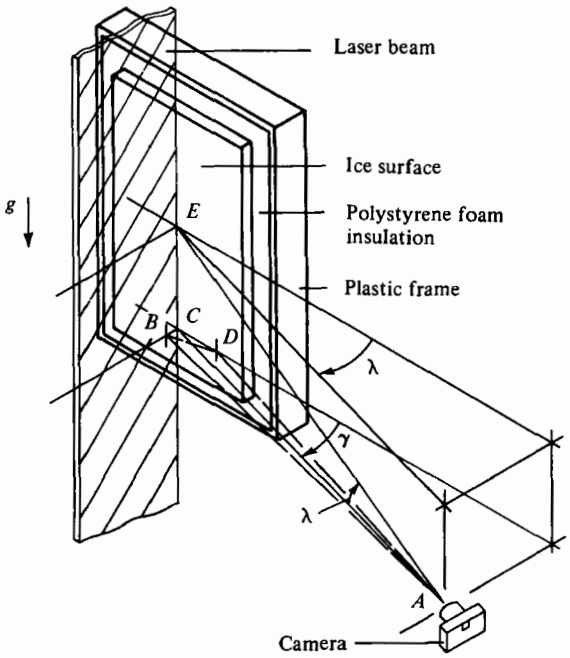

FIGURE 1. Schematic diagram showing the relative positions of the camera, ice surface and the laser beam.

The tank was filled to a depth of 80 cm with demineralized and de-ionized water. To visualize the flow, 0·75 g of Pliolite, ground to 40 μm size, was added to the water. Pliolite is a solid white resin manufactured by Goodyear Chemical Company which is used in coatings and adhesives. Pliolite is virtually insoluble in water and has a specific gravity of 1·026. The 40 μm particles remain suspended in water indefinitely. The horizontal beam of a 5 mW helium–neon laser was reflected off a first-surface mirror downward through a cylindrical lens which spread the beam in one direction. The spread beam, now approximately 2 by 60 mm in cross-section, continued down into the tank. Side scatter of the laser light off the pliolite particles made them visible.

The tank was surrounded by 7·6 cm of fibreglass insulation which, for the lowest water temperature considered here, limited the bulk temperature rise of the water in the tank to less than 0·03 °C per hour. Prior to each experiment, the tank temperature was reduced to the desired level, t_∞, using a circulating chiller. The tank water was stirred for 15 minutes after the chiller was removed to eliminate any non-uniformity in temperature. The tank was then allowed to stand for 40 minutes to let viscous effects damp out the residual motion from the stirring.

After preparing the tank and equilibrating the ice slab to 0 °C, the frame surrounding the ice slab was attached to a support fixture and the slab at the end of the assembly was slowly lowered into the tank. The support fixture was pre-adjusted so that, when the slab was fully submerged, the ice surface was vertical to within $\pm 2°$ and the laser beam was aligned perpendicular to the ice surface. When a section of the insulation surrounding the tank was removed, the particles in the beam could be seen through the glass walls of the tank. The ice was allowed to melt for approximately

5 minutes after immersion, allowing transient effects to die out. Using a motor-driven 35 mm Nikon camera, controlled by a Nikon intervalometer, sequential photographs were taken of the flow. The intervalometer was programmed to take several time exposures in succession, with the shutter closed for a prescribed time interval between exposures. The length of the time exposure and the interval between photographs could be controlled by the intervalometer to an accuracy of $\pm 0{\cdot}05$ s. A running clock was started when the ice was immersed, and the time at the beginning of each sequence of time exposures was recorded. This made it possible to compute the elapsed time between any two photographs taken while the ice slab melted.

The relative positions of the ice slab, the light beam and the camera may be seen in figure 1: note that the camera's line of sight is at a small angle λ to the plane of the ice surface. The camera was positioned in this manner intentionally to determine the position of the ice surface in the photographs of the flow. To align the camera precisely along the ice surface would be difficult to do accurately and would require continual adjustment since the ice surface recedes as it melts. At small angles λ the viewer at point A in figure 1 will see the streak due to particle B directly and he will also see the reflected image of B at point D in the ice surface. For these small angles, the position of the ice surface in the plane of the beam, at point C in figure 1, can be accurately determined by bisecting the angle BAD. This amounts to simply bisecting the distance in the photograph between the streak lines near the surface and their respective reflected images. Thus the position of the ice interface can be determined from the photographs without adjusting the camera position. The distance between the camera and the plane of the light beam was recorded for each experiment and used to correct distances measured from the photographs for azimuthal (λ) and altitude (γ) angle effects. Photographs were taken for a range of ambient water temperatures, as discussed in the next section.

3. Results and discussion

Figures 2 and 3 show a time-exposure photograph of the flow occurring at each of the ambient temperature conditions considered here, from 3·90 to 8·40 °C, that is, from $R = -0{\cdot}033$ to $R = 0{\cdot}520$. The length of the time exposure and the ambient temperature corresponding to each photograph are indicated. Note that near the surface in each photograph the streaks made by the particles form a pattern which is symmetric about a vertical line. This is because the camera sees both the particle itself and its reflexion in the ice surface. This line of symmetry at various points is found by bisecting the distance between the direct image of the streak and its reflexion. This marks the position of the ice–water interface in the plane of the light beam. The reference wires at the left-hand edge of each photograph are exactly 1·0 cm apart, indicating the physical scale of the flow. The side vertical edge of the ice toward the camera has a bright, mottled appearance which comes from the light striking the top of the ice surface, extending 9 mm away from the support frame. The light penetrates the ice and is, in part, scattered by air bubbles frozen deep below the surface of the ice.

The sequence of photographs in figures 2 and 3 shows clearly the transition from total upflow, at $t_\infty = 3{\cdot}9$ °C, to total downflow, at $t_\infty = 5{\cdot}9$ °C and also at 8·4 °C. At $t_\infty = 3{\cdot}9$ °C the buoyancy force is totally upward, producing the simple upward

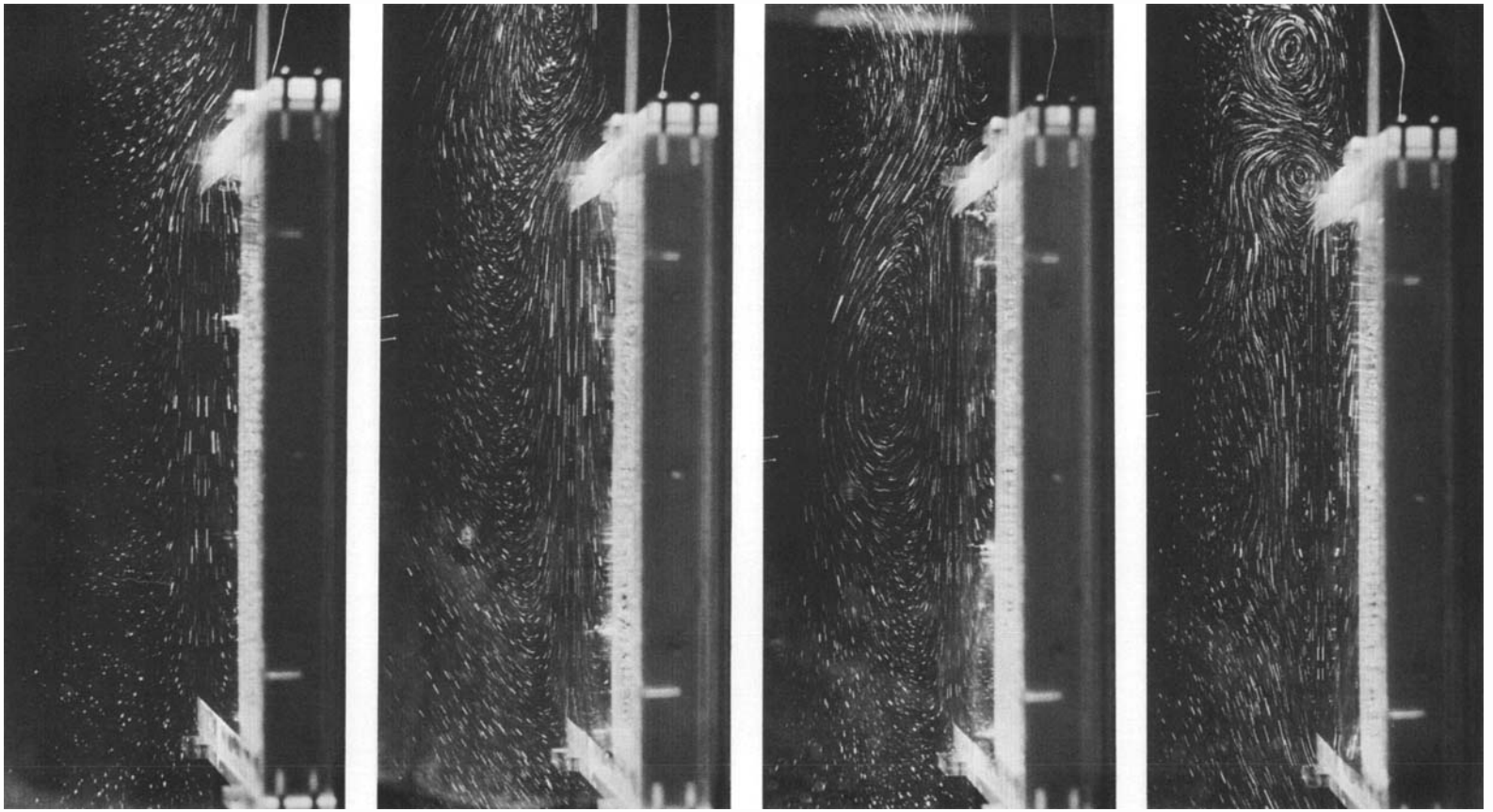

(*a*) (*b*) (*c*) (*d*)

FIGURE 2. Flow adjacent to a vertical ice slab melting in pure water. The corresponding ambient temperatures, R values, and exposure times are: (*a*) 3·90 °C, $R = -0{\cdot}033$, 6 s; (*b*) 4·05 °C, $R = 0{\cdot}005$, 10 s; (*c*) 4·40 °C, $R = 0{\cdot}084$, 10 s; (*d*) 4·70 °C, $R = 0{\cdot}143$, 10 s. The reference wires at the left edge of each photograph are 1 cm apart.

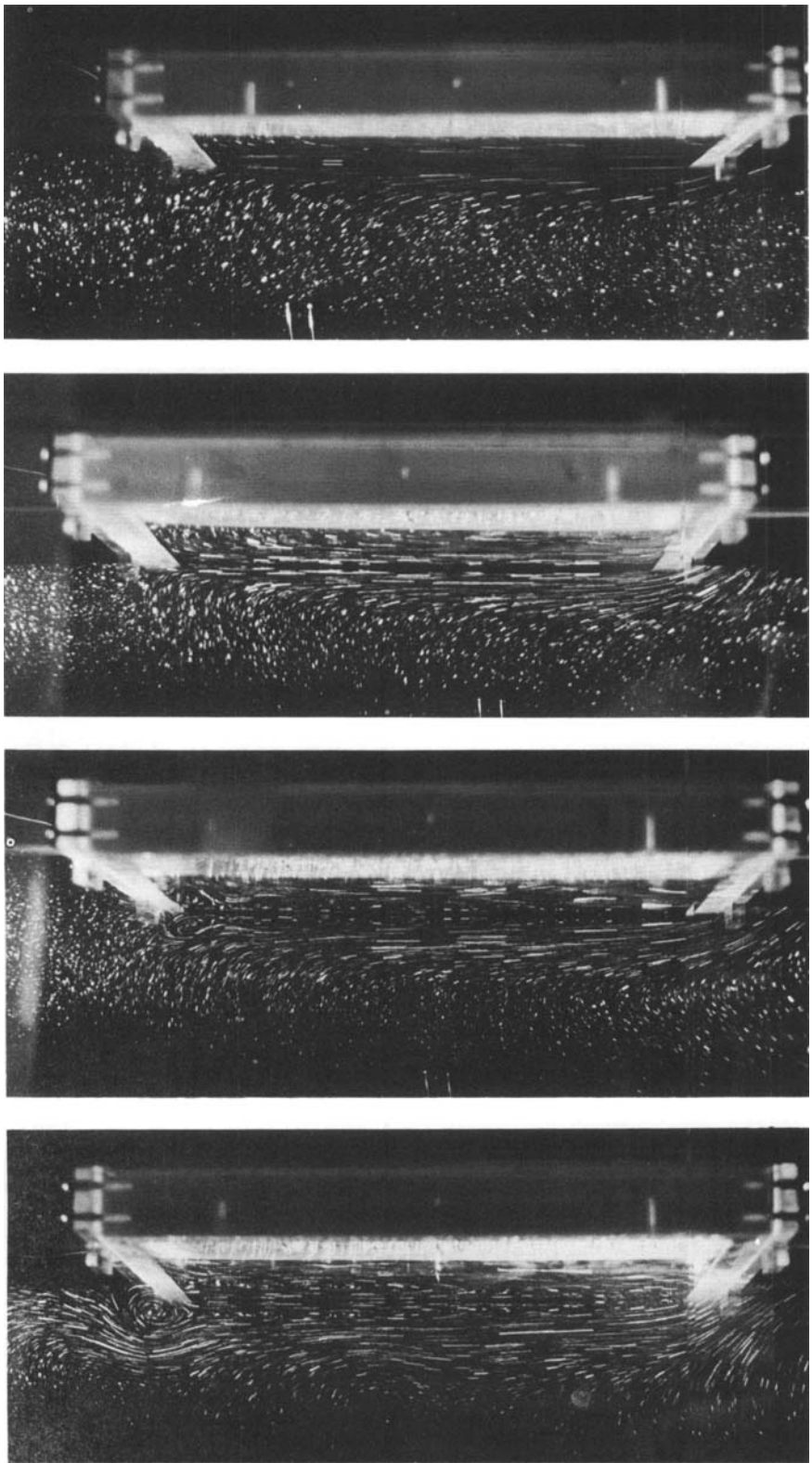

FIGURE 3. Flow adjacent to a vertical ice slab melting in pure water. The corresponding ambient temperatures, R values, and exposure times are: (*a*) 5·00 °C, R = 0·194, 10 s; (*b*) 5·40 °C, R = 0·254, 10 s; (*c*) 5·90 °C, R = 0·317, 10 s; (*d*) 8·40 °C, R = 0·520, 6 s. The reference wires at the left edge are 1 cm apart.

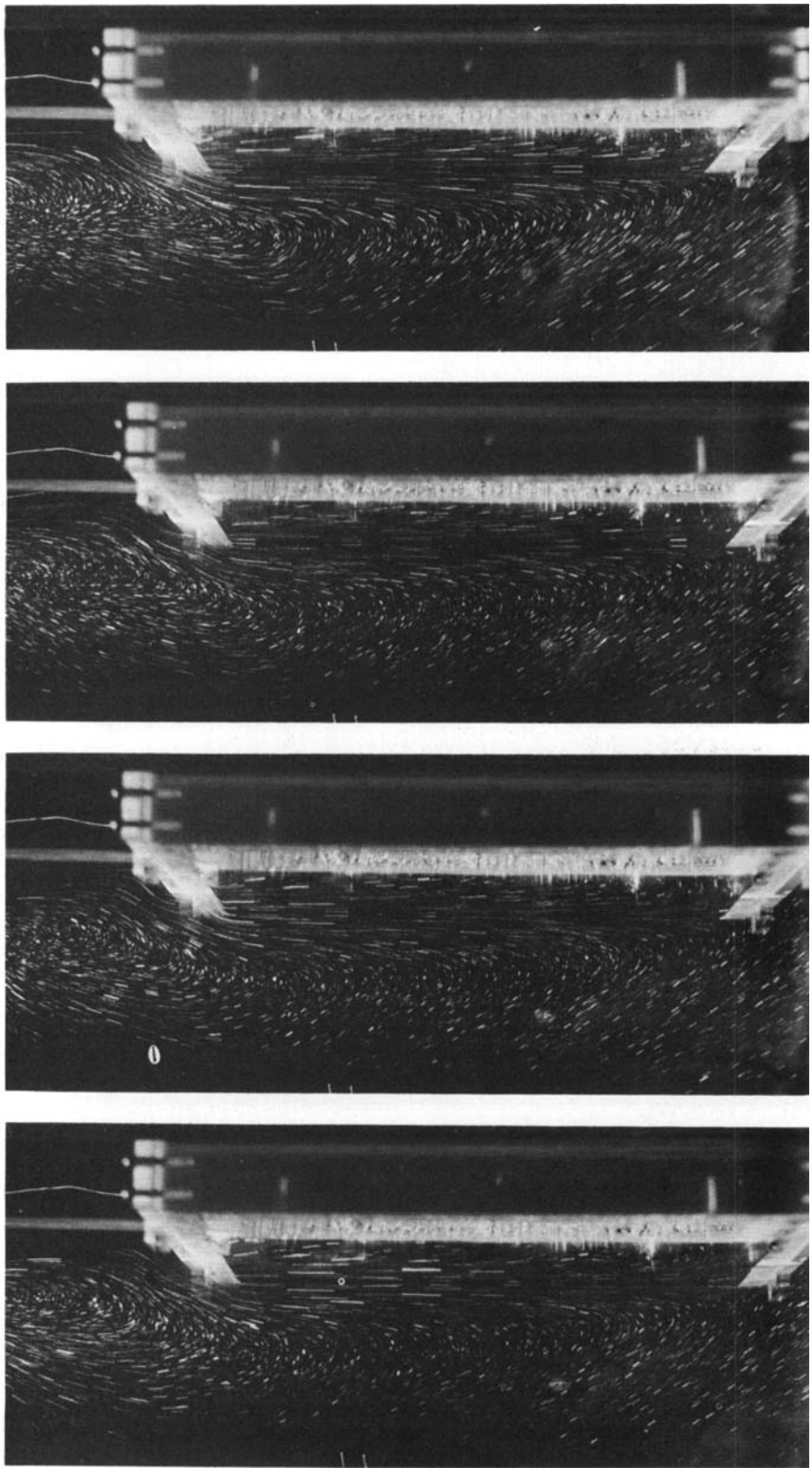

FIGURE 4. Flow adjacent to a vertical ice slab melting in pure water at 4·05 °C (R = 0·005). The four photographs are 10 second time exposures taken in sequence (from left to right) with the shutter closed for 30 s between frames. The reference wires at the left edge are 1 cm apart.

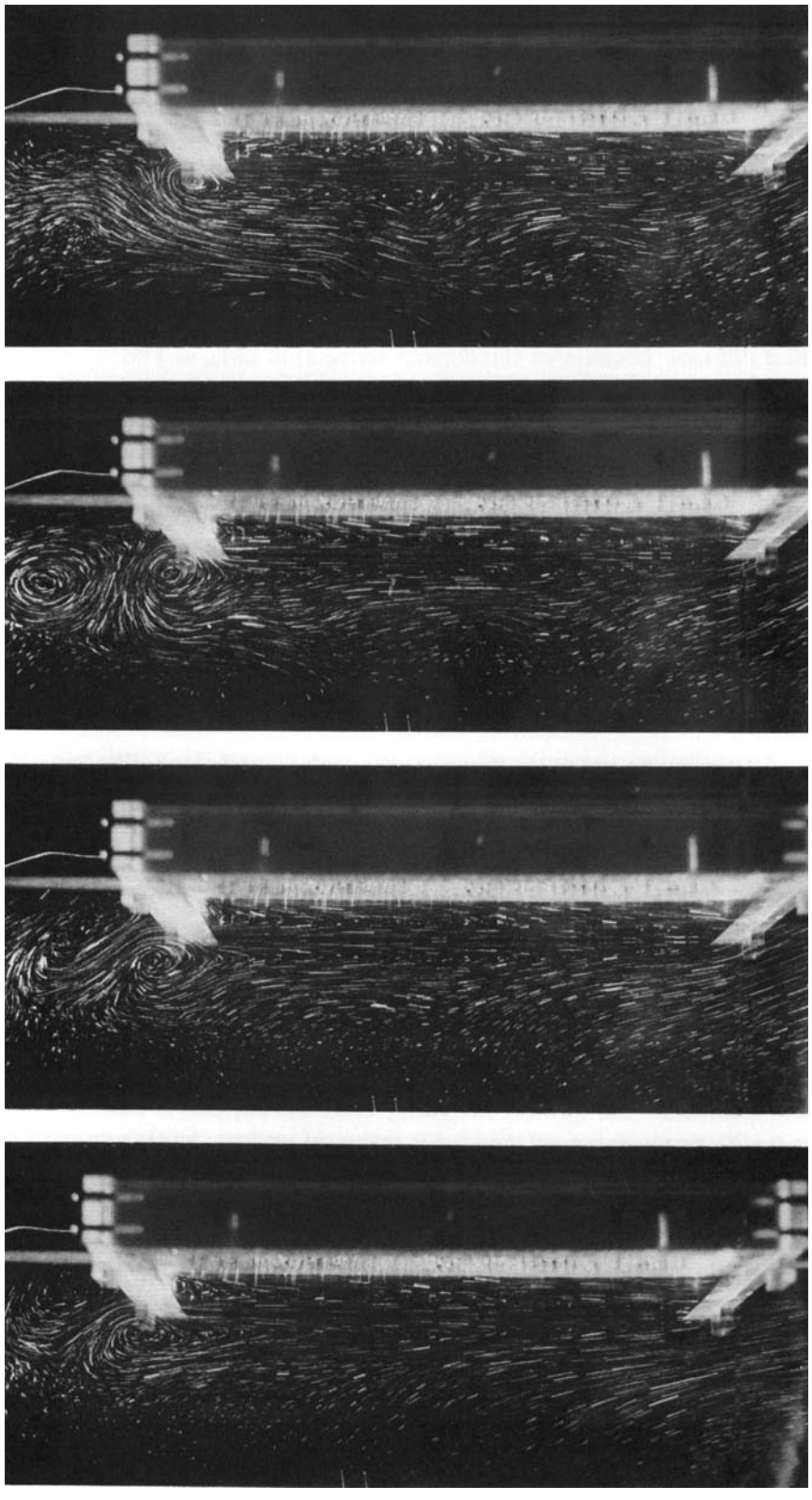

FIGURE 5. Flow adjacent to a vertical ice slab melting in pure water at 4·40 °C (R = 0·084). The four photographs are 10 second time exposures taken in sequence (from left to right) with the shutter closed for 30 s between frames. The reference wires at the left edge are 1 cm apart.

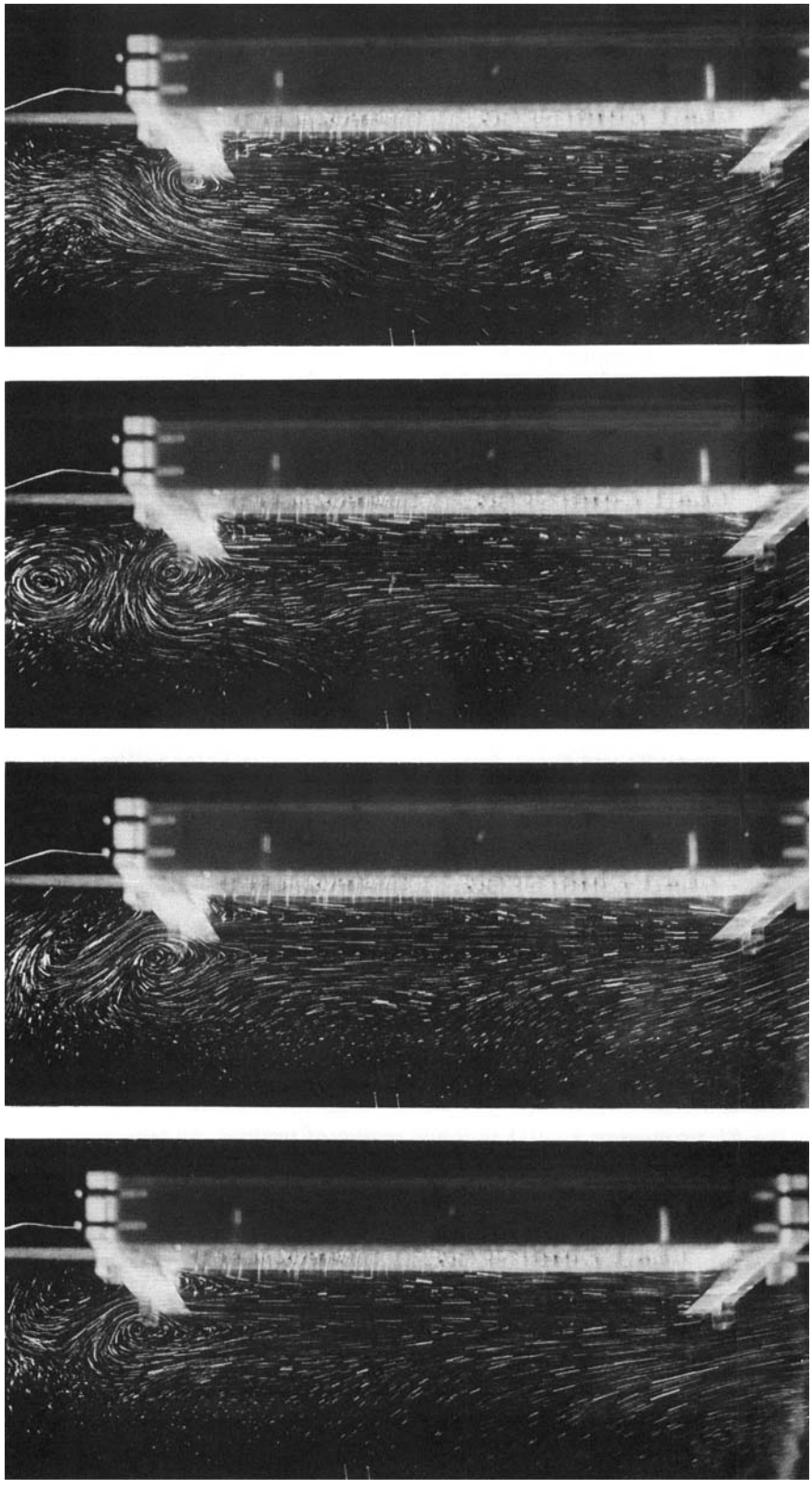

(*a*) (*b*) (*c*) (*d*)

FIGURE 6. Flow adjacent to a vertical ice slab melting in pure water at 4·70 °C (R = 0·143). The four photographs are 10 second time exposures taken in sequence (from left to right) with the shutter closed for 30 s between frames. The reference wires are 1 cm apart.

boundary-layer flow seen in figure 2(*a*). Note that fluid is entrained from the ambient in the left-hand portion of the photograph. At 4·05 °C, the flow near the surface is upward and boundary layer in character, and there is a weak downward flow at the outer edge of the boundary layer. A sequence of time exposures for $t_\infty = 4{\cdot}05$ °C is shown in figure 4, demonstrating that the weak outside downflow is not a transient feature, but a characteristic of the steady-state flow. Figure 4 suggests that the wake above the ice slab is the source of the outside downflow. This was confirmed by visual observations of the wake region during the experiment. The temperature of the fluid leaving the upper edge of the ice surface is between 0 °C and $t_\infty = 4{\cdot}05$ °C. Since both sides of the ice slab are melting, the wakes from each side join to form a single buoyant jet. As this fluid moves upward, it is mixed with entrained ambient fluid and the thermal deficit diffuses. Because of the density extremum at $t_m = 4{\cdot}03$ °C, the fluid which is warmed to near t_m is denser than the ambient. Negative buoyancy then acts to decelerate and move some of this fluid downward. Some of the cold fluid in the wake travels upward until it reaches the air–water interface, 35 cm above the top edge of the slab. This fluid in turn forms a thin colder layer at the top of the tank. Through conduction and mixing, some of this fluid warms to near t_m, whereupon it too begins to move downward, eventually feeding the weak downflow at the outer edge of the upward boundary layer near the ice surface. The downflow is therefore due to warming of the fluid in the shed wake and, to a lesser degree, to warming of the cold wake fluid which collects at the air–water interface. Since laminar jets are known to become unstable at small downstream distances, it is not surprising that figure 4 shows some weak variation of the outside flow with time, particularly near the upper edge.

At $t_\infty = 4{\cdot}4$ °C (figures 2*c* and 5) the flow near the surface again looks like boundary-layer flow, but away from the surface a stronger downward flow exists which, together with the upward flow, forms a single almost cellular pattern. Sequential photographs for $t_\infty = 4{\cdot}4$ °C in figure 5, indicate some weak variation of the outside flow pattern with time. However, the basic flow pattern remained unchanged during the experiment. The mechanism producing the outside downward flow is the same as that for $t_\infty = 4{\cdot}05$ °C, except that the downward buoyancy force for fluid in the wake warmed to t_m is stronger for $t_\infty = 4{\cdot}4$ °C. The outside downward flow for $t_\infty = 4{\cdot}4$ °C is also stronger than for $t_\infty = 4{\cdot}05$ °C, as seen in figure 2. Again, the instability of the wake causes the weak time variation of the outer flow.

For $t_\infty = 4{\cdot}7$ °C and 5·0 °C (figures 2*d*, 3*a* and 6) the flow takes on a different character. For these conditions the upward buoyancy near the surface is weaker than at $t_\infty = 4{\cdot}05$ or 4·4 °C, producing a smaller inner region of upflow. As this upward flow leaves the top surface of the ice, only a very short distance is required for the outer part of the flow to become sufficiently warm, through mixing and diffusion, that the buoyancy force becomes negative. The outer portion of the upward wake flow then decelerates and reverses direction. This produces a standing vortex at the top edge of the ice, as seen in figures 2(*d*) and 3(*a*). Since the back side of the ice slab is also melting, a vortex rotating in the opposite direction forms at the top of the back ice surface. These two vortices interact with the unstable wake above the slab to produce the time-varying flow field seen in figure 6. (Note the secondary vortex seen in figure 6(*c*).) Remnants of other similar secondary vortices produce a wavering of the outer downflow which can be seen in some of the remaining frames. Apparently

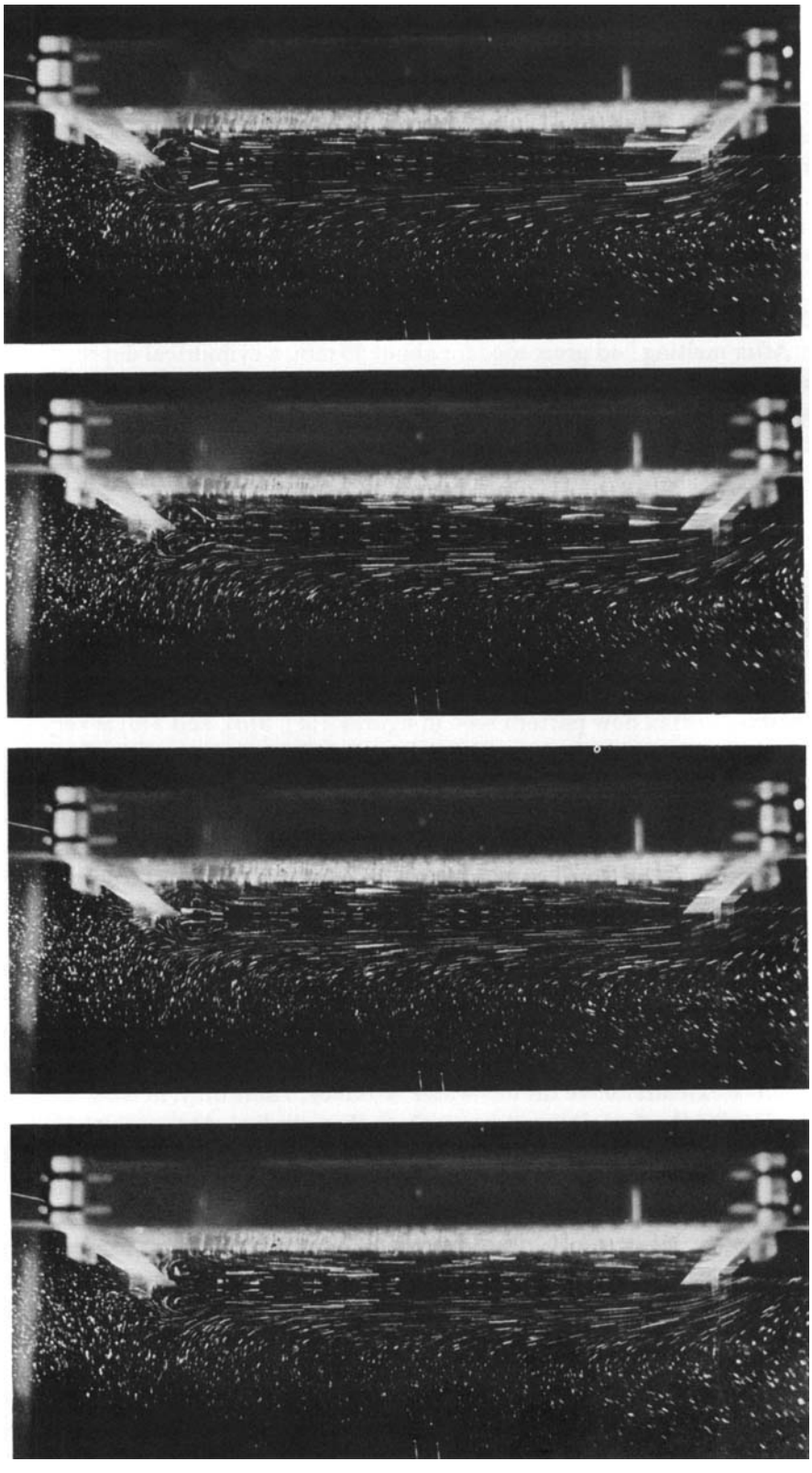

FIGURE 7. Flow adjacent to a vertical ice slab melting in pure water at 5·40 °C (R = 0·254). The four photographs are 10 second time exposures taken in sequence (from left to right) with the shutter closed for 30 s between frames. The reference wires are 1 cm apart.

these vortices are generated in the wake region and, although they slowly dissipate, they are convected downward in the outer flow, causing the outer flow to be unsteady.

At $t_\infty = 5{\cdot}40$ °C (figures 3*b* and 7) the upward flow near the surface is very weak. A small vortex is visible at the top of the ice surface. Only a short distance beyond the upper edge of the ice is needed to reverse the buoyancy force acting on all the fluid in the upward wake. Unlike the flows at lower ambient temperatures, no fluid escapes upward. All the upward flow quickly decelerates and begins moving downward, feeding a strong downward flow outside the upward flow near the surface. No significant time-dependent behaviour is detectable in figure 7. In addition to being smaller, the standing vortex is also located lower than those observed at $t_\infty = 4{\cdot}70$ and 5·00 °C. At $t_\infty = 5{\cdot}40$ °C the vortex is adjacent to the ice surface just below the top edge. After melting had proceeded for about 25 min, a cylindrical depression in the ice surface about 1 mm deep could be seen at the location of the vortex. Apparently the presence of the vortex enhanced the local melt rate, producing the depression horizontally across the ice slab.

At 5·90 °C, despite a bi-directional buoyancy force, a totally downward flowing boundary layer is observed in figure 3(*c*). There is no detectable upward flow at all near the surface, even though the buoyancy force there is upward. As pointed out by Carey *et al.*, for these conditions ($R = 0{\cdot}317$) the effect of the upward buoyancy near the surface is strongly inhibited by the large viscous forces there. The flow direction is therefore dictated by the effect of the downward buoyancy farther from the surface. At $t_\infty = 8{\cdot}40$ °C, the buoyancy force is entirely downward and, as seen in figure 3(*d*), this also results in purely downward boundary-layer flow.

The standing-vortex flow pattern seen in figures 2(*d*), 3(*a*), and 3(*b*) is very similar to the streamlines in a sketch drawn by Schecter & Isbin (1958) of the flow pattern observed at the top of an electrically heated plate in cold water. The configuration of the trailing edge of the heated surface is slightly different from that at the top of our ice surface. However, the mechanisms and resulting flow pattern were found to be essentially the same. Our findings also agree, for the most part, with those of Wilson & Vyas (1979). There were, however, some diffcrences. At 4·40 °C, our photographs clearly indicate an outer downward flow whilst Wilson & Vyas detected none. There are two reasons for this difference. First, their 22 mm wire electrode is so short that our photographs indicate it would not detect most of the downward flow which we observe at 5·0 cm above the bottom edge of the ice. Secondly, and probably most important, the interaction with the wake does not occur in their experiment because their ice surface extends above the air–water interface. There may, in fact, be no outer downward flow for the flow circumstances which they studied. At $t_\infty = 5{\cdot}9$ °C Wilson & Vyas found a weak upward flow near the surface and also found the flow to be time dependent. We found neither the upflow nor significant time dependence. We can only speculate that the presence of the air–water interface may be affecting their flow to produce the different results. The differences seen in these two studies further emphasize the role played by the wake interaction in controlling the flow behaviour.

In addition to showing the general flow features, the photographs provide quantitative information about both the flow velocities and the local heat-transfer rates. To determine the velocities at various points in the flow, the following technique was used. On a full-scale photograph of any given flow, the distance between pairs of images near the ice surface was bisected. This was done at several vertical locations

and a line was drawn connecting them so that the position of the ice surface was known at all downstream locations. The projected length of a particle streak parallel to the ice surface was then measured with a precision scale. The velocity parallel to the ice surface was computed by dividing the measured length by the length of the time exposure and correcting for the small-angle optical effects discussed in the previous section. Likewise, the distances from the centre of the streak to the leading edge and to the ice surface were measured and corrected for small-angle effects. The streak lengths and positions were measured to an accuracy of $\pm 0{\cdot}25$ mm. The measured velocities were thereby accurate to within $\pm 2\,\%$ of the maximum velocity in the flow. The velocity and position measurements were then converted to the similarity variables of Carey *et al.* with the following relations:

$$f' = \frac{ux}{2\nu(Gr_x)^{\frac{1}{2}}}, \quad \eta = \frac{y}{x}(Gr_x/4)^{\frac{1}{4}}, \tag{1), (2}$$

$$Gr_x = \frac{gx^3}{\nu^2}\alpha(s_\infty, p)\,|t_0 - t_\infty|^q. \tag{3}$$

Here x and y are the downstream and surface-normal co-ordinates and u is the velocity parallel to the surface. The constants g and ν are the gravitational acceleration and kinematic viscosity, respectively, and $\alpha(s_\infty, p)$ and q are constants from the density relation of Gebhart & Mollendorf (1977). Following Carey *et al.*, different co-ordinate systems are used above and below $R = 0{\cdot}20$. For $R < 0{\cdot}20$, the leading edge is taken at the bottom of the ice surface with u and x positive in the upward direction. For $R > 0{\cdot}20$, the leading edge is taken at the top of the ice surface with u and x positive downward.

The resulting data for the flows with large regions of upflow ($R < 0{\cdot}20$) are plotted in figure 8 and the symbols corresponding to each ambient temperature level are listed in table 1. Also shown in figure 8 are the computed results of Carey *et al.* These results are shown for pure water for $R = 0$, $0{\cdot}10$ and $0{\cdot}14$, with $Pr = 11{\cdot}6$, which is approximately an average value of Pr for the range of temperatures considered here. The calculations do not include the interface blowing effect resulting from melt addition. However, as shown by Carey *et al.*, such effects are small at these low ambient temperatures and may be neglected.

At $t_\infty = 3{\cdot}90$ °C, the measured velocities are in excellent agreement with the theoretical predictions over the entire flow region. At $t_\infty = 4{\cdot}05$ °C agreement is good over most of the profile. However, at about $\eta = 2{\cdot}0$ the experimental data points deviate and at large η become negative, reflecting the outside downflow observed in the photographs. Similarly, at $t_\infty = 4{\cdot}40$ °C and $t_\infty = 4{\cdot}70$ °C near the surface the data agrees well with the theory, but the experimental results are too low at larger η. At large η the measured velocities are negative and the similarity observed at smaller η breaks down. As pointed out previously, the downflow at large η for these conditions is a consequence of the wake reversing direction, moving downward and interacting with the upward flow near the surface. The theoretical calculations are based on a semi-infinite plate and therefore could never predict this outside downflow. The agreement near the surface is important since, for the large $Pr = 11{\cdot}6$, the thermal transport region is close to the surface, and therefore mostly in the region where theory and experiment agree. This suggests that the surface heat transfer predicted

t_∞ (°C)	R	Pr_f	Symbols
3·90	−0·033	12·26	⬣ ⬢
4·05	0·005	12·22	⊙ ●
4·40	0·084	12·15	◇ ◆
4·70	0·143	12·08	▽ ▼
5·40	0·254	11·93	◹ ◤
5·90	0·317	11·82	⊡ ■
8·40	0·520	11·30	△ ▲

TABLE 1. The ambient temperatures at which velocity measurements were taken and the corresponding transport parameters and symbols used in figures 8 and 9. The solid and line symbols denote data taken at different times as the ice melted.

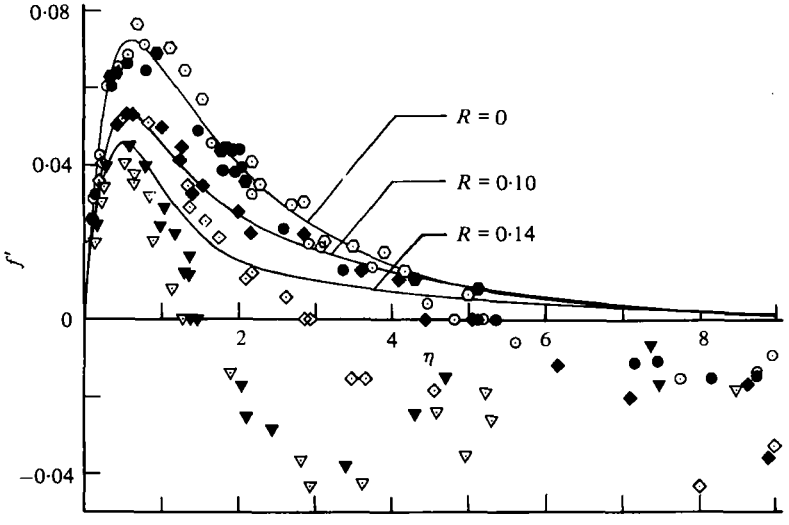

FIGURE 8. Measured velocity profiles for ambient water temperatures below 5 °C. The conditions corresponding to each symbol are listed in table 1. Also shown are the theoretical velocity profiles (——) for various values of R for Pr = 11·6, q = 1·894816 from Carey, Gebhart & Mollendorf (1980).

by the theory may be accurate despite the fact that the predicted velocity is totally unrepresentative at large η. We recall that near the surface the profiles did not vary with time in any given experiment.

For the downward flows ($R > 0{\cdot}20$) the measured and calculated velocities are similarly shown in figure 9. The computed profiles from Carey *et al.* are for pure water for R = 0·30, 0·32, 0·40 and 0·50, with Pr = 11·6. At t_∞ = 5·90 and 8·40 °C the experimental results agree very well with the computed profiles. Carey *et al.* did not succeed in calculations for t_∞ = 5·40 °C. However, the similarity transformation is seen in figure 9 to collapse the data for t_∞ = 4·40 °C remarkably well.

The photographs of the flow field were also used to compute the local heat transfer. In two photographs of the flow taken at different times during the experiment, the position of the ice–water interface was determined by bisecting the streak pairs. In

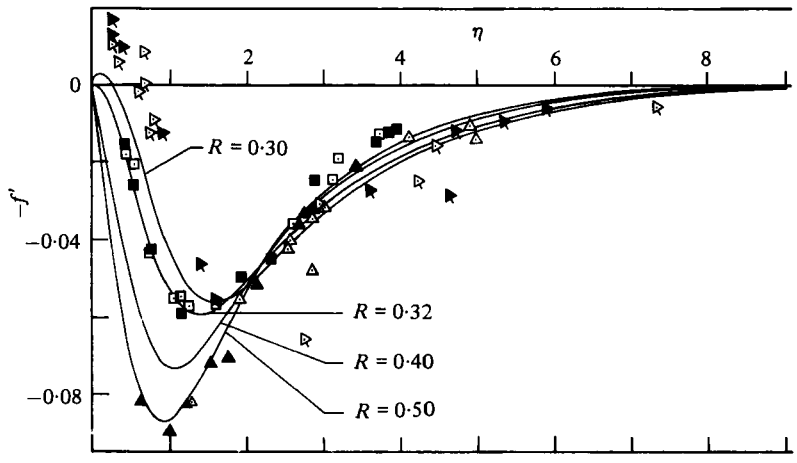

FIGURE 9. Measured velocity profiles for ambient water temperatures above 5 °C. The conditions corresponding to each symbol are listed in table 1. Also shown are the theoretical velocity profiles (——) for various values of R for $Pr = 11{\cdot}6$, $q = 1{\cdot}894816$ from Carey *et al.* (1980).

both photographs, the distance from the end of the lower reference wire to the ice–water interface was measured along a line normal to the interface. The difference in the measured distances yields the melting rate in the interval between photographs. Using the latent heat for ice to calculate the heat transfer, the following relation is obtained which relates the local Nusselt number to the measured quantities:

$$Nu_x Gr_x^{-\frac{1}{4}} = \frac{h_x x}{k} Gr_x^{-\frac{1}{4}} = \left[\frac{x}{Gr_x^{\frac{1}{4}} k}\right]\left[\frac{\Delta l}{\Delta \tau}\right]\left[\frac{\rho_i h_{il}}{t_\infty - t_0}\right]. \tag{4}$$

Here h_x is the local heat transfer coefficient, k is the thermal conductivity of water, ρ_i is the density of ice, h_{il} is the specific heat of fusion of ice, and Δl and $\Delta \tau$ are the measured changes in distance and time between photographs, respectively. For the resulting data points see figure 10. Because the interface moves only a small distance in the time intervals considered here, the accuracy of the heat transfer data is limited by the accuracy of the distance measurement to only about $\pm 20\,\%$. Nevertheless, the measurements in figure 10 agree well with the previous data and the theory of Carey *et al.* For $R < 0{\cdot}20$, as discussed above, for the velocity measurements, the measured heat transfer agrees with the values predicted by the theory despite the large differences in the velocity profiles at large η seen in figure 8.

4. Conclusions

The time-exposure photographs presented here document the nature of the natural convection flow adjacent to a vertical ice surface melting in pure water at ambient water temperatures between 3·9 and 8·4 °C. For t_∞ between 4·05 and 5·40 °C, part or all of the upward flow leaving the top edge of the ice surface warms and reverses direction, moving downward and interacting with the upward flow near the surface. For $t_\infty = 4{\cdot}05$, 4·40 and 4·70 °C this interaction causes the outer flow field to depart significantly from that predicted by the similarity solutions of Carey *et al.* for a semi-

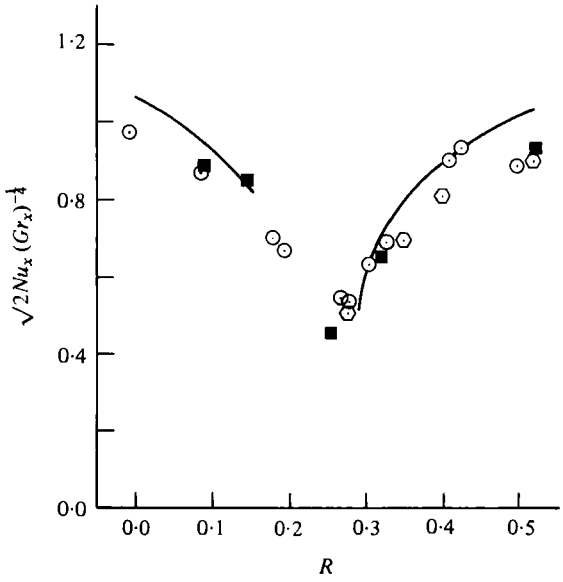

FIGURE, 10. Measured heat transfer data: ■, present study; ⊙, Bendell & Gebhart (1976); ⊙, Johnson (1978). Also shown is the theoretical heat-transfer curve (——) for ice melting in fresh water obtained by interpolating the results of Carey *et al.* (1980).

infinite vertical ice surface. However, near the surface the effect of this outer downflow is weak and there is still good agreement between the measured and theoretical velocity profiles. The surface heat transfer inferred from the measured melt rates agrees well with that predicted by the similarity solutions. This is to be expected since the high Prandtl number ($Pr \cong 11{\cdot}6$) implies that the thermal transport occurs principally in a region very close to the surface, where the flow field agrees with that predicted by the similarity solution. The weak time dependence seen in some of these flows is believed to be due to an instability of the shed wake above the ice slab. This is the source of the outside downflow. At $t_\infty = 5{\cdot}9$ and $8{\cdot}4$ °C the measured velocity profiles and heat transfer are found to agree well with those predicted by the similarity solutions.

The flow patterns in figures 2 and 3 also indicate that the method used by Bendell & Gebhart to predict flow direction will not yield correct results in some instances. Using thermocouples at the top and bottom of the ice slab, one might assume that the flow direction is always towards the colder thermocouple. At $t_\infty = 5{\cdot}40$ °C the top thermocouple would detect the cold fluid in the small vortex near the top of the ice surface, whereas the bottom junction would detect the downward wake which is warmer because of entrained ambient fluid. Thus, it would be concluded that the flow is upward. In fact all the upward flow reverses at the top and feeds the larger downward outer flow, see figure 3(*b*). From the flow patterns observed in figures 2 and 3 it is difficult to determine exactly the conditions for convective inversion, i.e. where the flow changes from predominantly upflow to predominantly downflow. It is nevertheless now clear that the conditions for convective inversion cannot accurately be determined using pairs of thermocouples. The most accurate statement which may be made about convective inversion from the present results is that, as

t_∞ increases, the flow changes from predominantly upflow at $t_\infty = 4{\cdot}40$ °C to predominantly downflow at $t_\infty = 5{\cdot}40$ °C. These conditions are $R = 0{\cdot}084$ and $R = 0{\cdot}254$, respectively. For $4{\cdot}05\ °C < t_\infty < 5{\cdot}90\ °C$ the flow is bi-directional and, for some conditions, time dependent.

These results compare favourably with the values predicted by the analysis of Carey *et al.* Total convective inversion was predicted to occur between $t_\infty = 4{\cdot}75$ and 5·81 °C. The computations indicate bi-directional flow between $t_\infty = 4{\cdot}75$ and 5·98 °C. For an ice surface of finite length, the wake reversal has resulted in bi-directional flow for a wider range of t_∞ than is predicted by the analysis. The analysis assumes a semi-infinite surface and therefore the wake behaviour is not taken into account.

The flow field observed for $4{\cdot}05\ °C \leqslant t_\infty \leqslant 5{\cdot}40\ °C$ departs strongly from simple boundary-layer flow because of the reversal of part or all of the upward wake. Any complete model of the flow for these conditions must account for the manner in which the wake returns to interact with the upward flow near the surface.

Van P. Carey wishes to acknowledge graduate fellowship support from the Woodburn Foundation. The authors also wish to acknowledge support for this study by the National Science Foundation under research grant ENG77-21641.

REFERENCES

Bendell, M. S. & Gebhart, B. 1976 Heat transfer and ice melting in ambient water near its density extremum. *Int. J. Heat Mass Transfer* **19**, 1081–1087.

Carey, V. P., Gebhart, B. & Mollendorf, J. C. 1980 Buoyancy force reversals in vertical natural convection flows in cold water. *J. Fluid Mech.* **97**, 279–297.

Gebhart, B. & Mollendorf, J. C. 1977 A new density relation for pure and saline water. *Deep-Sea Res.* **24**, 813–848.

Gebhart, B. & Mollendorf, J. C. 1978 Buoyancy-induced flows in water under conditions in which density extrema may arise. *J. Fluid Mech.* **89**, 673–707.

Johnson, R. S. 1978 Transport from a melting vertical ice slab in saline water. M.S. thesis, State University of New York at Buffalo.

Josberger, E. G. 1979 Laminar and turbulent boundary layers adjacent to melting vertical ice walls in salt water. *Sci. Rep.* no. 16. Office of Naval Research.

Schecter, R. S. & Isbin, H. S. 1958 Natural-convection heat transfer in regions of maximum fluid density. *A.I.Ch.E. J.* **4**, 81–89.

Vanier, C. R. & Tien, C. 1968 Effect of maximum density and melting on natural convection heat transfer from a vertical plate. *Chem. Eng. Prog. Symp. Series* **64**, 240–254.

Wilson, N. W. & Vyas, B. D. 1979 Velocity profiles near a vertical ice surface melting into fresh water. *Trans. A.S.M.E. J. Heat Transfer* **101**, 313–317.